The Role of the Stratosphere in Teleconnections Arising From Fast and Slow MJO Episodes

Priyanka Yadav[1,2,3] ![ORCID], **Chaim I. Garfinkel**[4] ![ORCID], **and Daniela I. V. Domeisen**[1,5] ![ORCID]

[1]ETH Zurich, Zurich, Switzerland, [2]ESSIC, University of Maryland, College Park, MD, USA, [3]Now at UMD/ESSIC, NASA/GSFC, Greenbelt, MD, USA, [4]The Hebrew University of Jerusalem, Fredy and Nadine Herrmann Institute of Earth Sciences, Edmond J. Safra Campus, Jerusalem, Israel, [5]Université de Lausanne, Lausanne, Switzerland

Abstract The Madden-Julian Oscillation (MJO) can influence the extratropical circulation on timescales up to several weeks, with a dependence on the MJO characteristics: MJO episodes that propagate slowly across the Maritime Continent have a stronger impact on Euro-Atlantic weather than fast MJO episodes. While the tropospheric pathway for MJO teleconnections with varying phase speeds is well understood, in this study, we investigate the contribution of the Northern Hemisphere stratospheric pathway for fast versus slow MJO episodes. During slow MJO episodes, Phases 5–6 lead to increased upward wave propagation in the North Pacific sector, and subsequently enhanced heat flux at 100 hPa, leading to the weakening of the polar vortex. The results suggest a clear role of stratosphere-troposphere coupling for slow MJO episodes, which is proposed as a mechanism for anomalously strong positive polar cap height anomalies in MJO Phases 7–8.

Plain Language Summary The Madden-Julian Oscillation (MJO) consists of an eastward-moving band of clouds, rainfall, and winds in the tropics. The MJO originates over the West Indian Ocean and typically takes 10–20 days to propagate from the Indian Ocean (Phase 3) to the Western Pacific (Phase 6). The convection associated with the MJO influences global weather via wave-propagation. The waves propagate through both a tropospheric and stratospheric pathway. The MJO is, therefore, an important source of mid-latitude predictability on timescales of weeks to months. Here, we explore the stratospheric pathway, differentiating between fast and slowly propagating MJO episodes. Slowly propagating MJO episodes significantly strengthen the polar vortex from day 0–18 following Phases 3–5 and weaken the vortex following Phases 7–8. The weakening of vortex is due to a strengthening of the low-pressure system in the North Pacific sector, allowing upward wave propagation into the stratosphere during Phases 6–1. This weakened vortex signal then propagates into the troposphere causing persistent warm anomalies in the polar cap region. Fast MJO episodes show a weaker response than slow cases. Our study suggests that slowly propagating MJO episodes have the potential to extend the predictability of the stratosphere and its subsequent impact on the North Atlantic region.

1. Introduction

Tropical diabatic heating anomalies associated with convective anomalies from the Madden-Julian Oscillation (MJO) can significantly impact global weather on subseasonal-to-seasonal timescales (Lin, 2022; Matthews, 2004). The MJO propagates eastward with an average propagation speed of 5 ms^{-1} from the East Indian Ocean to the central Pacific Ocean and circumnavigates the globe with a period of 30–90 days (Waliser et al., 2009; Zhang, 2005). During boreal winter, the tropical diabatic heating associated with the MJO generates poleward and eastward propagating Rossby wave trains that influence global weather patterns. The MJO is thus an important remote driver of extreme temperature and precipitation events across the globe on subseasonal timescales and is considered a major source of subseasonal predictability for global weather (Domeisen et al., 2022; Lin, 2022; Stan et al., 2017; Vitart, 2017).

Observational and modeling studies have shown that the MJO can influence the North Atlantic Oscillation (NAO) via both tropospheric and stratospheric pathways (Cassou, 2008; Garfinkel et al., 2014; Schwartz & Garfinkel, 2017, 2020). Enhanced MJO convection over the tropical Indian Ocean and reduced convection in the tropical Pacific (MJO Phases 2–3) lead to a significant increase in the probability of occurrence of the positive NAO phase (hereafter +NAO) at a lag of 10 days or more (Cassou, 2008; Lin et al., 2009). On the other hand, MJO convection over the western Pacific, that is, Phases 6–7 of the MJO, lead to an increase in the occurrence

Writing – original draft: Priyanka Yadav

Writing – review & editing: Priyanka Yadav, Chaim I. Garfinkel, Daniela I. V. Domeisen

of the negative NAO phase (hereafter −NAO) at lags of 10–15 days (Cassou, 2008; Lin et al., 2009). In addition to this tropospheric pathway, the MJO can also influence the NAO via a stratospheric pathway through poleward and vertical propagation of quasi-stationary waves (Garfinkel et al., 2012; Garfinkel et al., 2014; F. Wang et al., 2018; Yang et al., 2019; Kang & Tziperman, 2018). The influence of the MJO on the stratosphere is observed as a weakening (strengthening) of winds and a decrease (increase) in polar cap geopotential height anomalies in the lower stratosphere and upper troposphere after Phases 6–7 (2–3) (Garfinkel et al., 2014). As a first step in this pathway, the Aleutian low, a climatological low-pressure system over the North Pacific (hereafter NP), strengthens via constructive interference with the MJO-induced anomalies after MJO Phases 6–7. This region of amplified low pressure leads to an increase in upward wave propagation from the troposphere into the stratosphere, eventually weakening the polar vortex and warming of the stratosphere. In particular, a deepened climatological Northeast Pacific (hereafter NEP) low at 190°-220°E strengthens upward propagation of wave-1 heat flux into the stratosphere (Garfinkel et al., 2010). The MJO Phase 2–3 leads to the opposite response, consisting of a decrease in upward wave flux, which in turn results in a cooler stratosphere and a stronger stratospheric polar vortex. The stratospheric anomalies induced by the MJO teleconnections can in turn affect the state of the NAO (Barnes et al., 2019; Garfinkel et al., 2014). The NAO response to the MJO tends to be significantly stronger and longer lasting if the stratospheric pathway is present. For example, the strong cycle of the MJO in January and February 2018 has been cited as a precursor to the subsequent sudden stratospheric warming (SSW) event (Butler et al., 2020), which led to intense cold air outbreaks across Europe (Knight et al., 2021). Overall, 12 out of 23 SSW events between January 1979 and January 2013 were preceded by a strong MJO Phase 6 or 7 (Schwartz & Garfinkel, 2017).

The studies mentioned above are based on the mid-latitude response to the MJO heating in a particular phase when all strong MJO days are pooled together. However, the MJO has a diverse nature: while a canonical MJO event propagates eastward at an average propagation speed of 5 ms⁻¹, individual MJO events differ strongly in their eastward propagation speed. MJO events defined as slow (fast) move at an average speed of 3.9 (6.4) ms⁻¹ with a period of 65 (36) days (Yadav et al., 2019) from Phase 1 to Phase 8. Slow events have a longer residence time over the Maritime Continent (Phases 4–5). Thus the heating and cooling associated with individual MJO events induce different time-lagged Rossby wave responses than the response observed by compositing all MJO events (Yadav & Straus, 2017; B. Wang et al., 2019). In the case of slowly propagating MJO episodes, a robust +NAO regime occurs 15 days after Phase 4 (Yadav & Straus, 2017), whereas a +NAO regime follows Phases 2–3 at a 15-day lag when all strong MJO episodes are considered (Cassou, 2008). A strong −NAO develops a week after Phase 6 in slow episodes which persists through Phase 8. Fast MJO episodes lead to the development of a comparatively weak +NAO after Phases 2–3 and −NAO after Phases 6–7 at 15 days lag. Overall, the remote response for slowly propagating MJO episodes exhibits a stronger NAO response than fast MJO episodes (Yadav & Straus, 2017; Yadav et al., 2019). The MJO Phases are used as predictors for the state of the polar vortex and the NAO, hence a better understanding of the MJO teleconnection pathways is important to reduce uncertainty in the attribution of time-lagged relationships of MJO teleconnections to different MJO Phases (Barnes et al., 2019; Ferranti et al., 2018; Schwartz & Garfinkel, 2020; Stan et al., 2022; Yadav & Straus, 2017).

The tropospheric pathway for teleconnections from MJO events with varying propagation speeds is well understood. However, the stratospheric pathway for MJO events of fast and slowly propagating MJO events has not yet been explored, although the stratosphere has been shown to be an important factor in modulating the response to MJO events in the extratropics. In particular, it is not understood if the stronger impact of slow MJO episodes on the North Atlantic region is due to a potential stratospheric pathway of the slow MJO episodes or if the slow MJO pathway is a direct tropospheric pathway. In this study, we investigate the potential stratospheric pathway during fast and slow MJO episodes using reanalysis data.

2. Data and Methods

Daily ERA-Interim reanalysis data (Dee et al., 2011b) for the period of 1980–2019 is used for analysis. In addition, the NOAA interpolated Outgoing Longwave Radiation (OLR) data set is used for computing MJO indices (Liebmann & Smith, 1996).

2.1. MJO Diagnostics

For the diagnosis of the MJO, multivariate EOF analysis (described in Wheeler and Hendon (2004)) is applied to filtered anomalies of zonal wind at 850 and 200 hPa, and OLR averaged between 15°N and 15°S for the period of
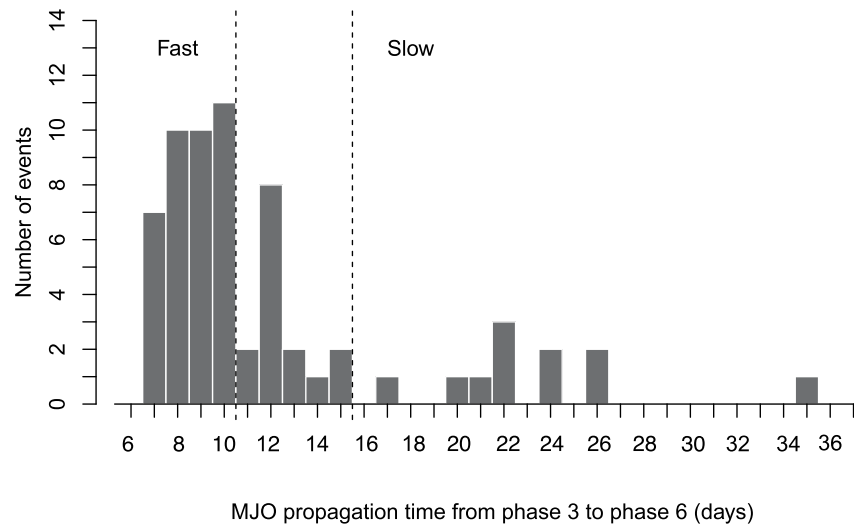
Figure 1. Histogram of the number of MJO episodes as a function of the propagation time (in days) from Phase 3 to Phase 6. Cases when the MJO amplitude is greater than 1 for at least three consecutive days in both Phases 3 and 6 of an MJO cycle are considered. The *y*-axis indicates the number of identified episodes in the reanalysis data set. Dashed lines denote the limits for fast and slow MJO cases. The first bar shows a propagation time of 7 days.

1980–2019. The filtered anomaly fields for the input of the EOF analysis are calculated by first computing daily anomalies by removing the time mean and the first four harmonics and applying a 201-point Lanczos bandpass filter to retain intraseasonal variability (for details see W. Wang et al. (2014); Yadav and Straus (2017)). The first two leading EOFs represent the eastward propagation of the MJO. The MJO amplitude is calculated from the normalized time series of the two leading principal components, PC1 and PC2, defined as $\sqrt{(PC1^2 + PC2^2)}$, the phase angle is computed as arctan($PC1/PC2$).

2.2. Classification of MJO Episodes

The classification of slow and fast MJO cases depends on the propagation time of the MJO from the Indian Ocean (Phase 3) to the western Pacific (Phase 6). In this study, we are considering cases when the MJO is active in Phase 3 and subsequently in Phase 6 in a cycle. Another criterion applied here is that the MJO amplitude has to be greater than 1 for at least three consecutive days in both Phase 3 and Phase 6 for each MJO episode considered in the analysis (following Yadav and Straus (2017)). Figure 1 shows a histogram of the number of episodes as a function of the propagation time (in days) of the MJO episodes from Phase 3 to Phase 6. Slow MJO episodes are defined as cases for which the MJO takes more than 15 days to propagate from Phase 3 to Phase 6. Note that Yadav and Straus (2017) used 20 days instead of the here used 15-day threshold, though we find that lowering the threshold to 15 days adds only one slow case and the geopotential height response is similar to the study by Yadav and Straus (2017) for slow cases with a propagation time of 20 days (see Figure 1). Fast cases are defined as cases for which the MJO takes 10 days or less to propagate from Phase 3 to Phase 6. To have a clear distinction between fast and slow cases, MJO cases that take between 11 and 15 days are not considered in the analysis. Eleven slow cases and 38 fast cases are identified using this classification. A list of the slow and fast cases and the dates for co-occurring SSW events during the MJO episodes are provided in Table 1.

2.3. Composite Analysis and Significance Testing

The period from October to March 1980/1981–2018/2019 (i.e., 39 winters) is used for the composite analysis. Anomalies are computed by applying a 20–100 days bandpass filter to temperature, geopotential height, zonal wind, and wavenumber 1 and wavenumber 2 components of eddy heat flux ($v'T'$, where the primes denote the deviation from the zonal mean). Composites are then calculated for the area-weighted average of geopotential height anomalies at 500 hPa and 100 hPa for the NEP sector 35–55°N 190–220°E, wavenumber 1 and wavenumber 2 components of the eddy heat flux for 40–80°N, geopotential height anomalies at 100 hPa at lower stratosphere (Z100) and mid-troposphere 500 hPa (Z500) for 70–90°N, polar cap temperature anomalies (65–90°N),

Table 1
Start and End Dates of Slow and Fast MJO Episodes, and Corresponding SSW Events During the MJO Episodes

Fast MJO episodes

Start date	End date	SSW
1-Oct-1980	4-Nov-1980	–
20-Oct-1982	20-Nov-1982	–
26-Oct-1985	22-Dec-1985	–
23-Dec-1985	6-Feb-1986	–
21-Oct-1986	24-Nov-1986	–
25-Oct-1987	27-Nov-1987	–
28-Nov-1987	10-Jan-1988	8-Dec-1987
11-Jan-1988	26-Feb-1988	–
30-Dec-1988	14-Feb-1989	–
12-Oct-1990	30-Nov-1990	–
12-Dec-1991	18-Jan-1992	–
6-Jan-1993	23-Feb-1993	–
27-Jan-1994	4-Mar-1994	–
26-Dec-1994	1-Feb-1995	–
17-Nov-1996	5-Jan-1997	–
7-Nov-2000	22-Dec-2000	–
23-Dec-2000	3-Mar-2001	11-Feb-2001
24-Oct-2002	9-Dec-2002	–
10-Dec-2002	26-Jan-2003	18-Jan-2003
27-Nov-2003	13-Jan-2004	5-Jan-2004
16-Dec-2004	19-Jan-2005	–
1-Jan-2006	8-Feb-2006	21-Jan-2006
12-Dec-2006	8-Feb-2007	–
9-Feb-2007	13-Mar-2007	24-Feb-2007
21-Jan-2008	1-Mar-2008	22-Feb-2008
2-Mar-2008	31-Mar-2008	–
17-Jan-2009	16-Feb-2009	24-Jan-2009
26-Oct-2009	19-Dec-2009	–
11-Oct-2011	17-Nov-2011	–
18-Nov-2011	14-Dec-2011	–
14-Oct-2012	27-Nov-2012	–
30-Jan-2013	17-Mar-2013	–
12-Nov-2014	13-Dec-2014	–
13-Dec-2014	17-Jan-2015	–
28-Feb-2016	30-Mar-2016	–
16-Jan-2017	15-Feb-2017	–
30-Oct-2018	28-Nov-2018	–
6-Jan-2019	16-Feb-2019	–

Table 1
Continued

Slow MJO Episodes

Start Date	End Date	SSW
1-Nov-1984	21-Jan-1985	1 Jan 1985
23-Dec-1986	4-Mar-1987	23 Jan 1987
19-Jan-1992	17-Mar-1992	–
22-Nov-1993	7-Jan-1994	–
30-Jan-1998	23-Mar-1998	–
24-Oct-2001	7-Jan-2002	30 Dec 2001
8-Jan-2002	8-Mar-2002	–
20-Dec-2009	6-Feb-2010	9 Feb 2010
21-Oct-2015	6-Jan-2016	–
7-Jan-2016	28-Feb-2016	–
17-Feb-2018	31-Mar-2018	–

and 10 hPa zonal mean zonal wind anomalies at 60°N (U10). The statistical significance of MJO-related anomalies is evaluated by the following bootstrapping procedure. First, synthetic data sets are generated by resampling the full data set 1,000 times (with replacement) to test the significance of composites. Then, composites are computed based on the correct dates of the various episodes but using synthetic data sets. The percentage of times for which the absolute value of the observed anomaly composite (at a given grid point) exceeds those in the synthetic data sets provides the significance level.

3. Upward Troposphere-Stratosphere Coupling

We next show the tropospheric and stratospheric responses as composites for the eight MJO Phases during these 11 slow and 38 fast MJO episodes when the MJO amplitude exceeds 1. To better understand the upward stratospheric pathway for fast and slow MJO cases, we review in Figures S1 and S2 in Supporting Information S1 the 500 hPa geopotential height response for fast and slow cases in the NP sector already shown in Yadav and Straus (2017). We also superpose on these figures the full 500 hPa height field to highlight constructive and/or destructive interference (Garfinkel et al., 2010; Smith & Kushner, 2012). The negative height anomalies for days 0–8 (Figures S1 and S2 in Supporting Information S1) in the NP are collocated with the climatological low for fast cases (Figures S1e–S1h in Supporting Information S1) from Phases 5–8, thus strengthening the climatological low. Phases 2–4 lead to the opposite response. Interestingly for slow cases (Figure S2 in Supporting Information S1), the climatological NP low is enhanced from Phases 6–1, which is one phase later (Phase 6) than fast cases (Phase 5).

Next, we examine the height anomalies in the NEP sector and wave-1 and wave-2 meridional heat flux at 500 hPa and 100 hPa to understand the strengthening/weakening of upward wave propagation during the MJO Phases. A contemporaneous decrease in height anomalies from Phases 7–2 in fast cases (Figure 2a) strengthens the climatological trough in the NEP sector. This constructive interference with the climatological wave-1 trough leads to a significant increase in wave-1 500 hPa heat flux following Phases 6–1 (Figure 3a), and the destructive interference associated with a ridge in the NEP following Phases 4–5 leads to suppressed wave-1 heat flux from days 0–5. The wave-2 (Figure 3c) heat flux is enhanced in Phases 6–7.

This modulation of NEP height and of heat flux differs between slow and fast cases. A simultaneous anomalous decrease in NEP height (Figure 2b) is seen from Phases 7–2, similar to fast cases, but this decrease persists longer after Phases 6–8 in slow cases. This deepened NEP low in slow cases leads to enhanced wave-1 tropospheric heat flux anomalies (Figure 3b) from Phases 5–8. Namely, an MJO-induced low in the NEP sector enhances the heat flux via constructive interference with the climatological planetary waves (Garfinkel et al., 2012; Schwartz & Garfinkel, 2017; Smith & Kushner, 2012). The anomalies in wave-1 and wave-2 heat flux are generally of the same sign because the anomalous low is situated in the Northwestern Pacific, where the climatological station-
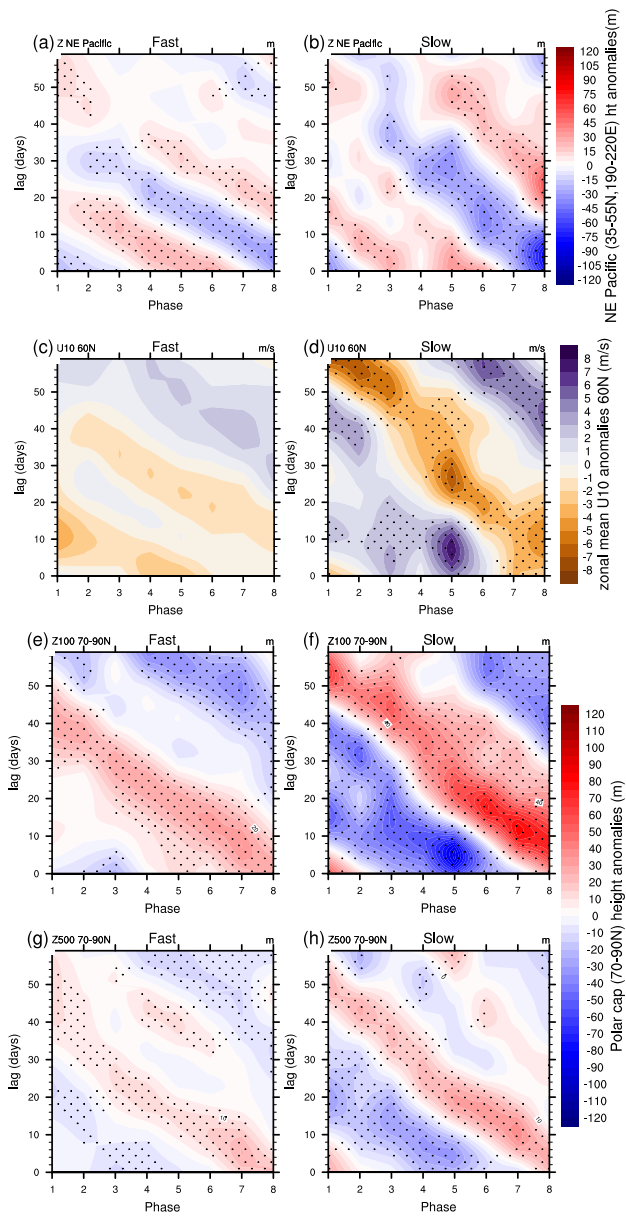
Figure 2. Geopotential height anomaly (units: m) composites of area-weighted average for the northeast Pacific (NEP) sector (35–55°N/180–220°E at 500 hPa (a, b); 10 hPa zonal mean zonal wind anomalies (units: m/s) at 60°N (U10) (c, d), polar cap height anomaly composites (units: m) for 70–90°N (Z100) at 100 hPa (e, f) and (Z500) 500 hPa (g, h) for fast and slow MJO episodes. The x-axis indicates the MJO phase and the y-axis is the lag in days with respect to each MJO phase. The contour interval is 5 m for height anomalies (a, b, e, f) and 1 m/s for U10 (c, d). Dots represent days with confidence levels above 95% using bootstrap resampling.

ary wave pattern for both wave-1 and wave-2 features a trough (Garfinkel et al., 2010).

MJO Phases 1–3 have a generally opposite response: slow MJO Phases 1–2 (Figures 3b and 3d) decrease the 500 hPa wave-1 tropospheric heat flux from days 0–24 and from days 0–10 after Phase 3. Fast MJO Phases 1–3 have a weaker and shorter-lived influence.

In the lower stratosphere (Figures 3f and 3h), a contemporaneous decrease in wave-1 heat flux anomalies is seen for slow cases from days 0–12 at 100 hPa for Phases 1–3 and for days 0–8 in Phase 5. Heat flux associated with wave-2 is suppressed up to day 30 following Phases 1–2. This suggests that the MJO convection in slow MJO cases in Phases 1–3 leads to less upward wave propagation, thereby reinforcing stronger vortex conditions in the lower stratosphere. This is evident from Figure 2d showing a strengthening of U10 at days 10–12 for Phases 1–2 and days 0–14 for Phases 3–5. Wave-1 heat flux is significantly enhanced from Phases 1–4 in fast cases, while enhanced wave-1 heat flux in slow cases is observed at 16–20 days lags following Phases 1–3.

At longer lags, that is, after the MJO-related NP teleconnection is established, the wave-1 slow case response is generally the opposite to fast cases (Figures 3e and 3f). Heat flux is enhanced starting at 15–20 days lag in the lower stratosphere for most Phases but with longer lead-times for Phases 1–2 than Phases 5–6. This enhanced heat flux leads to a weakening of the vortex (Figure 2d) and an anomalous increase in Z100 (Figure 2f). The difference in fast and slow cases is more striking for wavenumber 1 than wavenumber 2. Slow MJO cases lead to a longer-lasting wave pulse, and so the integrated heat flux is stronger, which tends to have a stronger effect on the vortex (Polvani & Waugh, 2004; Sjoberg & Birner, 2012). Wavenumber 1 heat flux anomalies are shown for the Pacific and Atlantic sectors in Figure S3 in Supporting Information S1. Interestingly, the heat flux in slow cases weakens in the Pacific sector following Phases 1–3 up to a lag of 10 days and is significantly enhanced after day 15. In the Atlantic sector, the heat flux first increases from days 0–20 and then decreases from day 20–38. The decrease in 100 hPa heat flux in slow cases (Figure 3f) from Phases 1–4 suggests a larger contribution of wavenumber 1 in slow MJO cases. This is likely due to the strong influence of the MJO on the NP (Figure S3 in Supporting Information S1), which more dominantly projects onto wavenumber 1 (Barriopedro & Calvo, 2014; Martius et al., 2009) if the height anomaly extends beyond the Northwest Pacific (Garfinkel et al., 2010).

We then examine the changes in the strength of the polar vortex for fast and slow MJO episodes for fast and slow MJO cases up to 60 days lag following the eight MJO Phases (Figures 2c and 2d). Slow cases (Figure 2d) lead to a significant increase in U10 from days 38–42 after Phases 1–2, and from days 8–20 following Phases 2–5. This increase is followed by a significant weakening of U10 after day 55 from Phases 1–3. In contrast to slow cases, the U10 response for fast cases is not significant and shows an anomalous decrease from Phases 1–3 (Figure 2c).

4. Downward Coupling to the Troposphere

We further investigate the downward impact of the stratosphere on the troposphere. We begin with the time evolution of polar cap temperature anomalies for each phase of the MJO in fast and slow MJO cases (Figure 4). In slow cases (row 2), an anomalously cold stratosphere is observed following Phases 1–3 from day 0–30. Strong
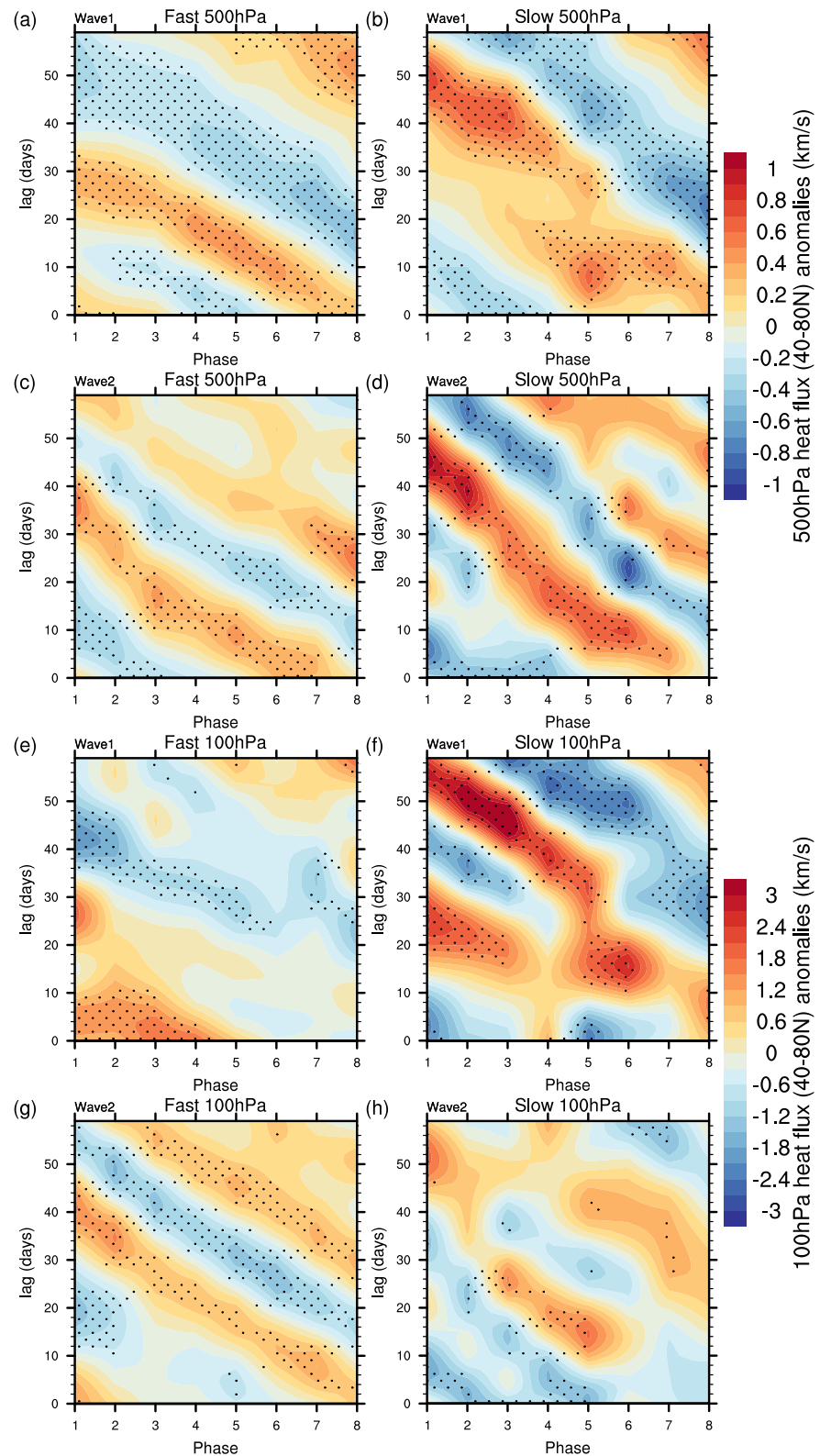
Figure 3. Anomalous heat flux (units: Km/s) at 500 hPa and 100 hPa for wavenumber 1 (a, b, e, f) and wavenumber 2 (c, d, g, h) area-weighted average from 40 to 80° for fast and slow MJO cases. The *x*-axis indicates the MJO phase and the *y*-axis is the lag in days with respect to each MJO phase. Dots represent days with confidence levels above 99% using bootstrap resampling.
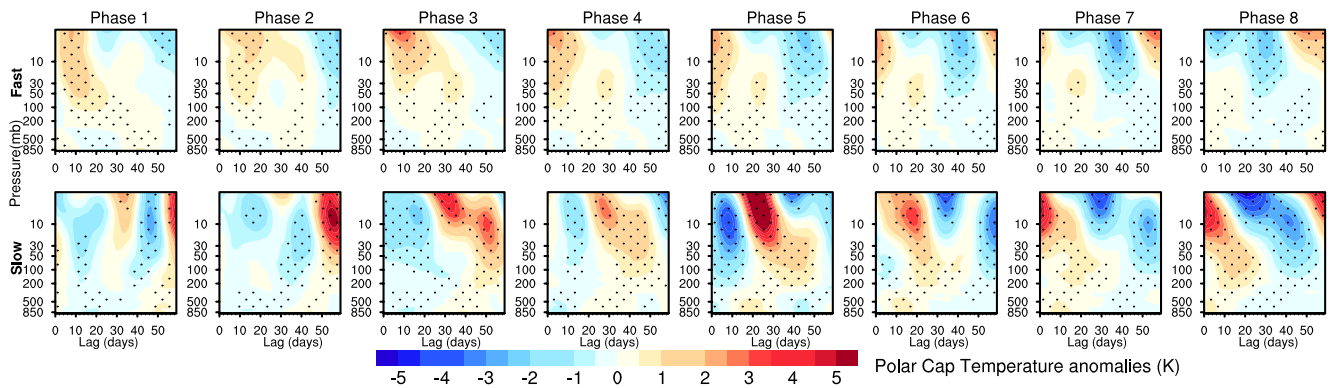
Figure 4. Polar cap temperature anomalies (area-weighted average of 65–90°N; units: K) for the 8 Phases of fast and slow MJO cases in rows 1 and 2, respectively. The *x*-axis indicates the lag in days with respect to the MJO phase from day 0–60. The *y*-axis is pressure in mb. Contour intervals are 0.5 K. Dots represent days with confidence levels above 99% using bootstrap resampling.

positive temperature anomalies begin to propagate downward 30 days after Phase 3 in slow MJO cases. The warmer anomalies enter the upper and mid-troposphere in Phases 6–8 of the MJO (Figure 4 and Figure S4 in Supporting Information S1). The temperature anomalies in the slow MJO cases extend to the lower troposphere and surface during Phases 7/8. The results strongly suggest a role of the stratosphere in slowly propagating MJO cases through a modulation of the polar vortex.

Anomalously warm stratospheric temperature in fast cases are found in the lower stratosphere around 20 days after MJO Phases 1–2. In contrast to slow cases, fast cases exhibit anomalously warm temperatures in the lower stratosphere around 20 days after MJO Phases 1–2 (Figure 4). This difference in the timing of the stratospheric downward impact between fast and slow cases may be attributed to the enhancement of heat flux following Phases 7–1 in fast cases and Phases 5–8 in slow cases (Figures 3a–3d).

The impact of the MJO heating in Phases 6–7 leads to a weakened polar vortex with respect to climatology and anomalously high stratospheric polar cap height (Schwartz & Garfinkel, 2020) when all MJO cases are considered. Based on the wind changes in U10 in Figures 2c and 2d, we studied corresponding changes in Z100 and Z500 (Figures 2e–2h) for fast and slow MJO episodes. In the lower stratosphere (Figure 2e,f), a significant decrease of Z100 occurs in Phases 1–4 for slow MJO cases after a 10-day lag. Fast cases show a decrease in Z100 for Phases 2–3 of the MJO up to an 8-day lag, and this decrease in Z100 is significant from days 0–5. Even though both fast and slow cases lead to an increase in Z100 after 10 days for Phases 6–8, the magnitude of the anomalies is three times larger for slow cases. In the mid-troposphere, fast MJO cases (Figure 2g) show a significant decrease in Z500 after Phases 1–3 at 15–22 days lag, where as slow MJO cases (Figure 2h) show a decrease in Z500 from Phases 1–4 even after a lag of 20 days. The negative height anomalies then transition to positive anomalies 10–20 days after Phases 5–7 in fast cases and after Phases 6–8 in slow cases. The positive anomalies in slow cases persist beyond 15 days during Phases 6–7 (Figure 2f). Fast cases do not show this persistence of positive anomalies that is observed for slow cases. The composite anomalies for slow cases show similar response for events with and without SSW at 10–20 days lag (Figure S5 in Supporting Information S1). The stratosphere has an integrative character, and hence a persistent forcing in slow episodes is more likely to solicit a response. A forcing that changes too quickly will not lead to a response that persists. Therefore, fast cases have a quickly decaying and weaker response.

The weakening of the vortex following MJO Phases 6–8 can contribute to a strong −NAO in slow cases. This is also evident in the Z100 and Z500 response to slow MJO cases (Figures 2f and 2h). This agrees with the finding of Yadav and Straus (2017), who have shown an increase in strong −NAO (+NAO) regime from Phases 6–8 (Phases 4–5). The MJO-induced changes in the polar vortex can drive the state of the NAO and give rise to a strong −NAO response in Phases 7–8 during slow MJO Phases. An increase (decrease) in Z100 in the lower stratosphere in slow cases reinforces a strong −NAO (+NAO) following phase 7–8 (4–5) in the troposphere. For fast cases, Z100 is positive from Phases 4–8 but the anomaly is short lived.

5. Conclusions

The aim of this study is to investigate the stratospheric pathway for MJO teleconnections with respect to fast and slowly propagating MJO episodes during northern hemispheric winter. Slow and fast MJO episodes are determined by the time they take to propagate over the Maritime Continent of the MJO. We define slow MJO episodes as episodes that take more than 15 days to propagate from the East Indian Ocean (Phase 3) to the Western Pacific (Phase 6). Fast MJO episodes are episodes when the MJO propagation time from Phase 3 to Phase 6 is 10 days or less.

This study demonstrates that the zonal phase speed of the MJO controls the strength and duration of the stratospheric teleconnection of the MJO. Slow MJO episodes strengthen the polar vortex in Phases 4–5, while strong upward wave activity during Phases 6–8 weakens the polar vortex. The duration of the heat flux pulse is longer for slow MJO cases than for fast cases, leading to a stronger impact on the vortex. Positive polar cap temperature anomalies start developing in the upper stratosphere after 30 days following Phase 3 of the MJO in slow cases. The signal starts propagating downward and impacts the surface during Phases 7–8. Fast MJO episodes show a weaker stratospheric response and positive anomalies develop in Phase 1.

The findings of this study will likely have implications for the extended-range predictability of midlatitude weather. In particular, long-lived and slowly propagating MJO episodes have the potential to extend the predictability of the stratosphere and the subsequent impact of the stratosphere on the North Atlantic region. In spite of limitations due to the small sample size of slowly propagating MJO cases, the study adds to our understanding of the stratospheric pathway and the behavior of the stratospheric impact on the surface due to the tropical heating associated with MJO episodes of varying phase speed.

Data Availability Statement

The ERA-Interim data (Dee et al., 2011b) is provided through the Copernicus Climate Change Service (C3S) Climate Data Store (CDS) (Dee et al., 2011a). The dates of SSW events for ERA-Interim were obtained from Butler et al. (2017). NOAA Interpolated Outgoing Longwave Radiation (OLR) data (Liebmann & Smith, 1996) is provided by NOAA PSL, Boulder, Colorado, USA.

References

Barnes, E. A., Samarasinghe, S. M., Ebert-Uphoff, I., & Furtado, J. C. (2019). Tropospheric and stratospheric causal pathways between the MJO and NAO. *Journal of Geophysical Research: Atmospheres*, *124*(16), 9356–9371. https://doi.org/10.1029/2019JD031024

Barriopedro, D., & Calvo, N. (2014). On the relationship between ENSO, stratospheric sudden warmings, and blocking. *Journal of Climate*, *27*(12), 4704–4720. https://doi.org/10.1175/JCLI-D-13-00770.1

Butler, A. H., Lawrence, Z. D., Lee, S. H., Lillo, S. P., & Long, C. S. (2020). Differences between the 2018 and 2019 stratospheric polar vortex split events. *Quarterly Journal of the Royal Meteorological Society*, *146*(732), 3503–3521. https://doi.org/10.1002/qj.3858

Butler, A. H., Sjoberg, J. P., Seidel, D. J., & Rosenlof, K. H. (2017). A sudden stratospheric warming compendium [Dataset]. *9*(1), 63–76. Earth System Science Data. https://doi.org/10.5194/essd-9-63-2017

Cassou, C. (2008). Intraseasonal interaction between the Madden–Julian oscillation and the North Atlantic Oscillation. *Nature*, *455*(7212), 523–527. https://doi.org/10.1029/2012GL053144

Dee, D. P., Uppala, S. M., Simmons, A. J., Berrisford, P., Poli, P., Kobayashi, S., et al. (2011b). The ERA-interim reanalysis: Configuration and performance of the data assimilation system [Dataset]. Quarterly Journal of the Royal Meteorological Society, *137*(656), 553–597. https://doi.org/10.1002/qj.828

Dee, D. P., Uppala, S. M., Simmons, A. J., Berrisford, P., Poli, P., Kobayashi, S., et al. (2011a). ERA-Interim global atmospheric reanalysis [Dataset]. Copernicus Climate Change Service (C3S) Climate Data Store (CDS). https://doi.org/10.24381/cds.f2f5241d

Domeisen, D. I. V., White, C. J., Afargan-Gerstman, H., Muñoz, Á. G., Janiga, M. A., Vitart, F., et al., (2022). Advances in the subseasonal prediction of extreme events: Relevant case studies across the globe. *Bulletin of the American Meteorological Society*, *103*(6), E1473–E1501. https://doi.org/10.1175/BAMS-D-20-0221.1

Ferranti, L., Magnusson, L., Vitart, F., & Richardson, D. S. (2018). How far in advance can we predict changes in large-scale flow leading to severe cold conditions over Europe? *Quarterly Journal of the Royal Meteorological Society*, *144*(715), 1788–1802. https://doi.org/10.1002/qj.3341

Garfinkel, C. I., Benedict, J. J., & Maloney, E. D. (2014). Impact of the MJO on the boreal winter extratropical circulation. *Geophysical Research Letters*, *41*(16), 6055–6062. https://doi.org/10.1002/2014GL061094

Garfinkel, C. I., Feldstein, S. B., Waugh, D. W., Yoo, C., & Lee, S. (2012). Observed connection between stratospheric sudden warmings and the Madden-Julian Oscillation. *Geophysical Research Letters*, *39*(18), L18807. https://doi.org/10.1029/2012GL053144

Garfinkel, C. I., Hartmann, D. L., & Sassi, F. (2010). Tropospheric precursors of anomalous Northern Hemisphere stratospheric polar vortices. *Journal of Climate*, *23*(12), 3282–3299. https://doi.org/10.1175/2010jcli3010.1

Kang, W., & Tziperman, E. (2018). The MJO-SSW teleconnection: Interaction between MJO-forced waves and the midlatitude jet. *Geophysical Research Letters*, *45*(9), 4400–4409. https://doi.org/10.1029/2018GL077937

Knight, J., Scaife, A., Bett, P. E., Collier, T., Dunstone, N., Gordon, M., et al. (2021). Predictability of European winters 2017/2018 and 2018/2019: Contrasting influences from the tropics and stratosphere. *Atmospheric Science Letters*, *22*(1). https://doi.org/10.1002/asl.1009

Liebmann, B., & Smith, C. A. (1996). Description of a complete (interpolated) outgoing longwave radiation dataset [Dataset]. *Bulletin of the American Meteorological Society*, *77*(6), 1275–1277. Retrieved from https://psl.noaa.gov/data/gridded/data.olrcdr.interp.html

Lin, H. (2022). The Madden-Julian Oscillation. *Atmosphere-Ocean*, *60*(3–4), 1–22. https://doi.org/10.1080/07055900.2022.2072267

Lin, H., Brunet, G., & Derome, J. (2009). An observed connection between the North Atlantic Oscillation and the Madden–Julian oscillation. *Journal of Climate*, *22*(2), 364–380. https://doi.org/10.1175/2008JCLI2515.1

Martius, O., Polvani, L. M., & Davies, H. C. (2009). Blocking precursors to stratospheric sudden warming events. *Geophysical Research Letters*, *36*(14). https://doi.org/10.1029/2009GL038776

Matthews, A. J. (2004). Atmospheric response to observed intraseasonal tropical sea surface temperature anomalies. *Geophysical Research Letters*, *31*(14), L14107. https://doi.org/10.1029/2004GL020474

Polvani, L. M., & Waugh, D. W. (2004). Upward wave activity flux as a precursor to extreme stratospheric events and subsequent anomalous surface weather regimes. *Journal of Climate*, *17*(18), 3548–3554. https://doi.org/10.1175/1520-0442(2004)017⟨3548:UWAFAA⟩2.0.CO;2

Schwartz, C., & Garfinkel, C. I. (2017). Relative roles of the MJO and stratospheric variability in North Atlantic and European winter climate. *Journal of Geophysical Research: Atmospheres*, *122*(8), 4184–4201. https://doi.org/10.1002/2016JD025829

Schwartz, C., & Garfinkel, C. I. (2020). Troposphere-stratosphere coupling in subseasonal-to-seasonal models and its importance for a realistic extratropical response to the Madden-Julian Oscillation. *Journal of Geophysical Research: Atmospheres*, *125*(10), e2019JD032043. https://doi.org/10.1029/2019JD032043

Sjoberg, J. P., & Birner, T. (2012). Transient tropospheric forcing of sudden stratospheric warmings. *Journal of the Atmospheric Sciences*, *69*(11), 3420–3432. https://doi.org/10.1175/JAS-D-11-0195.1

Smith, K. L., & Kushner, P. J. (2012). Linear interference and the initiation of extratropical stratosphere-troposphere interactions. *Journal of Geophysical Research*, *117*(D13), D13107. https://doi.org/10.1029/2012jd017587

Stan, C., Straus, D. M., Frederiksen, J. S., Lin, H., Maloney, E. D., & Schumacher, C. (2017). Review of tropical-extratropical teleconnections on intraseasonal time scales. *Reviews of Geophysics*, *55*(4), 902–937. https://doi.org/10.1002/2016RG000538

Stan, C., Zheng, C., Chang, E. K.-M., Domeisen, D. I. V., Garfinkel, C. I., Jenney, A. M., et al. (2022). Advances in the prediction of MJO teleconnections in the S2S forecast systems. *Bulletin of the American Meteorological Society*, *103*(6), E1426–E1447. https://doi.org/10.1175/BAMS-D-21-0130.1

Vitart, F. (2017). Madden—Julian Oscillation prediction and teleconnections in the S2S database. *Quarterly Journal of the Royal Meteorological Society*, *143*(706), 2210–2220. https://doi.org/10.1002/qj.3079

Waliser, D., Sperber, K., Hendon, H., Kim, D., Maloney, E., Wheeler, M., et al. (2009). MJO simulation diagnostics. *Journal of Climate*, *22*(11), 3006–3030. https://doi.org/10.1175/2008JCLI2731.1

Wang, B., Chen, G., & Liu, F. (2019). Diversity of the Madden-Julian Oscillation. *Science Advances*, *5*(7). https://doi.org/10.1126/sciadv.aax0220

Wang, F., Tian, W., Xie, F., Zhang, J., & Han, Y. (2018). Effect of Madden–Julian oscillation occurrence frequency on the interannual variability of northern hemisphere stratospheric wave activity in winter. *Journal of Climate*, *31*(13), 5031–5049. https://doi.org/10.1175/JCLI-D-17-0476.1

Wang, W., Hung, M.-P., Weaver, S. J., Kumar, A., & Fu, X. (2014). MJO prediction in the NCEP climate forecast system version 2. *Climate Dynamics*, *42*(9–10), 2509–2520. https://doi.org/10.1007/s00382-013-1806-9

Wheeler, M. C., & Hendon, H. H. (2004). An all-season real-time multivariate MJO index: Development of an index for monitoring and prediction. *Monthly Weather Review*, *132*(8), 1917–1932. https://doi.org/10.1175/1520-0493(2004)132<1917:aarmmi>2.0.co;2

Yadav, P., & Straus, D. M. (2017). Circulation response to fast and slow MJO episodes. *Monthly Weather Review*, *145*(5), 1577–1596. https://doi.org/10.1175/MWR-D-16-0352.1

Yadav, P., Straus, D. M., & Swenson, E. T. (2019). The Euro-Atlantic circulation response to the Madden-Julian Oscillation cycle of tropical heating: Coupled GCM intervention experiments. *Atmosphere-Ocean*, *57*(3), 161–181. https://doi.org/10.1080/07055900.2019.1626214

Yang, C., Li, T., Xue, X., Gu, S.-Y., Yu, C., & Dou, X. (2019). Response of the northern stratosphere to the Madden-Julian oscillation during boreal winter. *Journal of Geophysical Research: Atmospheres*, *124*(10), 5314–5331. https://doi.org/10.1029/2018JD029883

Zhang, C. (2005). Madden-Julian Oscillation. *Reviews of Geophysics*, *43*(2), RG2003. https://doi.org/10.1029/2004rg000158